Noninvasive Quantification of the Differential Portal and Arterial Contribution to the Liver Blood Supply From PET Measurements Using the ^{11}C-Acetate Kinetic Model

Sirong Chen* and Dagan Feng, *Fellow, IEEE*

Abstract—Our recent research has demonstrated that ^{11}C-acetate could be a complementary tracer to ^{18}F-fluorodeoxyglucose (FDG) in positron emission tomography (PET) imaging of hepatocellular carcinoma (HCC). In our previous modeling study, a three-compartment four-parameter model with a fixed contribution ratio of the liver's two blood supplies was proposed to characterize the kinetic behavior of ^{11}C-acetate in liver. However, in real pathology, both tumor and nontumor liver tissue can be heterogeneous in the distribution and proportion of the two blood supplies. To further improve the accuracy of quantitative analysis, the actual proportion of the hepatic artery and portal vein (PV) in different regions of interest (ROIs) was investigated in this study. An extra parameter a_v was included in the model input function to describe the contribution of PV to the liver. Ten ROIs extracted from six patients were used to test the models with fixed/nonfixed weighted dual-input function. The weighted nonlinear least squares algorithm was used to estimate all of the parameters. Evaluation of the adequacy of the two models was conducted and the computer simulation was performed to test the estimation accuracy of the new model. The forward clearance K was also estimated by the linear Patlak method. The results show that the model with parameter a_v in the input function was more suitable for mapping the tracer time activity curves. Moreover, the estimated a_v value fits the practical physiological and pathological conditions well and could be a potential candidate to provide useful additional diagnostic information for the early detection of hepatic metastases.

Index Terms—Dual-input function, noninvasive measurement, parameter estimation, positron emission tomography (PET), tracer kinetic modeling.

I. INTRODUCTION

HEPATOCELLULAR carcinoma (HCC) is the most frequent malignant tumor of the liver. Patients with HCC are often unaware of its presence until the tumor has reached an advanced stage [1] and less than 10% are cured with surgical resection. The overall five-year survival rate for late detection is less than 5% [2], [3]. It is important to detect HCC at its early stage for curative treatment. Positron emission tomography (PET) enables extracting quantitative physiological information *in vivo* from complex dynamic processes by using the tracer kinetic modeling techniques, which makes it useful for early detection of malignant tumors.

^{18}F-fluorodeoxyglucose (FDG) PET is well established for measurements of many physiological parameters. However, 40%–50% of HCC are not FDG-avid. Our recent research has demonstrated that ^{11}C-acetate could be a complementary tracer to FDG in PET imaging of HCC [4], [5]. To get a better understanding of the characteristics of ^{11}C-acetate in the imaging of HCC in the liver, quantitative dynamic modeling has been conducted [5], in which a three-compartment four-parameter (4P) model was presented and a new physiological parameter called "local hepatic metabolic rate-constant of acetate (LHMRAct)" was introduced to characterize the regional consumption of acetate by HCC and nontumor liver tissue. The tracer time-activity curve in blood (BTAC) was used as the model input function. To account for the liver's dual source of blood supply from the hepatic artery (HA) and portal vein (PV), we initially assumed a fixed contribution ratio of HA and PV in formulating the input function, viz. 20% contribution from HA and 80% from PV according to their approximate percentage perfusion to the nontumor liver tissue, 80% or 100% contribution from HA for HCC due to the generally accepted fact that the majority of the blood supply to established liver metastases is derived from the HA [1], [6], [7]. However, early stage metastases may not be easily differentiated on dynamic PET images, therefore, it may be difficult to choose the fixed weight for quantitative study. Furthermore, in real pathology, both the tumor and nontumor liver tissue can be heterogeneous in the distribution and proportion of the two blood supplies. Small liver tumors (<5 mm) are mainly fed by PV, while for larger tumors, these lesions receive up to 95% of their blood supply from HA [8]. For nontumor liver tissue, the two blood supplies may also vary within the liver and among individual patients due to many factors. Various liver diseases alter hepatic arterial circulation [9]. HCC is associated with liver cirrhosis in 80% of cases [6]; it is stated that normal liver parenchyma obtains about 75% of its blood supply from the PVs and 25% from the HAs, whereas in cirrhotic livers the blood supply

is obtained from the arteries in a proportion up to 75% [7]. The presence of regenerating and dysplastic nodules will also change the liver blood supply. Therefore, the fixed weighted dual-input function would increase the statistical uncertainties and reduce the accuracy in the estimated model parameters. The actual proportion of the two blood supplies in different regions of interest (ROIs) is needed to achieve more accurate quantitative analysis. In addition, measurement of the relative PV or HA contribution to liver blood flow might provide an alternative method for the detection of liver tumors [7].

Various kinds of methods have been used to distinguish PV and HA distribution. Direct measurements usually involve cannulation procedures which are very invasive and always performed on anaesthetized animals [10], [11]. Breedis and Young [12] injected dyes and plastic into the blood vessels for postmortem studies. Later, Lin *et al.* [13] used colored silicone rubber injected into the PV and HA to determine the different distribution. All of these techniques are too invasive to perform on humans. Alternative noninvasive techniques are, therefore, of great interest.

Sarper *et al.* [14] presented a noninvasive indirect measurement by using dynamic scintigraphy: measuring the first pass of an intravenous bolus injection of a radioactive colloid through the liver and kidney to obtain the hepatic perfusion index (HPI) from the time-activity curve (TAC) of the liver [7]. However, this technique is well recognized to be susceptible to numerous errors in the derivation of the index, such as the overlap of the hepatic arterial and portal venous phases and the presence of intrahepatic portosystemic shunting [7]. Chen *et al.* [15] has reported noninvasive quantification of hepatic arterial blood flow with nitrogen-13-ammonia and dynamic PET. All these techniques require extra examination and processing time and would cause more discomforts to the patients. Additionally, it is impossible to obtain the real-time PV and HA distribution during the PET scan.

In this study, we study the feasibility of including an extra parameter in the vascular input function of a ^{11}C-acetate liver model to obtain the differential portal and arterial contribution to the liver blood supply and evaluate the performance of this new modeling technique.

II. METHODS

A. Data Acquisition

The study population comprised six subjects, all of whom were hepatitis B carriers, including two with HCC. The transaxial (septa extended) dynamic PET images were obtained on an ECAT-EXACT 47 PET scanner (CTI/Siemens, Inc., TN, USA), which simultaneously recorded 47 contiguous planes. Each patient was positioned to allow image acquisition of the liver dome and apical half of the left ventricle to the inferior part of the liver. A Hanning filter was used for image reconstruction, resulting in an in-plane spatial resolution of 4.119 mm. The axial resolution was 3.375 mm.

Serial images were obtained immediately following bolus IV injection of ^{11}C-acetate. The dynamic sequence consisted of ten frames of 4 s, eight frames of 10 s, two frames of 30 s, three frames of 60 s, and two frames of 120 s, totaling 25 frames for a total scan time of 10 min.

B. Image Analysis

ROIs were defined using a single transverse slice of the full sets of dynamic ^{11}C-acetate images. Ten regions of dynamic datasets, two from HCC regions, others from nontumor liver regions, were extracted. In general, tracer kinetic modeling with PET requires the measurements of both BTAC and the tracer time-activity curve in tissue (TTAC) to quantitatively estimate the model parameters, using BTAC and TTAC as the input and output functions in the kinetic model. Although the arterial blood measurements are considered to be the most accurate representation of the BTAC and arterialized venous samples have been validated as a replacement of arterial samples [16], it is generally accepted that the insertion of arterial lines and the subsequent collection and processing of arterial blood are not compatible with the practice of clinical PET [17]. Moreover, it is highly invasive and virtually impossible in clinical settings to count the radioactivity of the portal venous blood by direct catheterization and sampling [5]. Therefore, in this study, the TACs of both HA and PV were evaluated using the image-derived method described in [5]. The PVs are small in size and not very distinguishable from the surrounding tissue, our newly proposed two-step segmentation method based on cluster analysis was also used to facilitate the extraction of the PV region [18].

C. ^{11}C-Acetate Liver Model With a Nonfixed Weighted Dual-Input Function

The ^{11}C-acetate liver model was shown in Fig. 1. The differential equations for the model are

$$\frac{d}{dt}c_e(t) = K_1 c_b(t) - (k_2 + k_3)c_e(t) \tag{1}$$

$$\frac{d}{dt}c_m(t) = k_3 c_e(t) \tag{2}$$

$$c_i(t) = c_e(t) + c_m(t) \tag{3}$$

where $K_1 - k_3$ are the rate constants, $c_b(t)$ is the ^{11}C-acetate concentration in the whole blood, $c_e(t)$ is the free ^{11}C-acetate concentration in intracellular space, $c_m(t)$ is the intracellular products/metabolites concentration, and $c_i(t)$ is the sum of $c_e(t)$ and $c_m(t)$. As seen in Fig. 1, another parameter hepatic blood volume (HBV) was included in the model to account for the contribution of the tracer within vascular/sinus space of the liver tissue to the observed total tissue activity; then the observed total tissue activity $c_T(t)$ is given by

$$c_T(t) = c_i(t) + \text{HBV} * c_b(t). \tag{4}$$

The solution of $c_T(t)$ in terms of macroparameters is

$$c_T(t) = (B_1 + B_2 e^{-L_1 t}) \otimes c_b(t) + \text{HBV} * c_b(t) \tag{5}$$

where

$$B_1 = \frac{K_1 k_3}{k_2 + k_3},$$
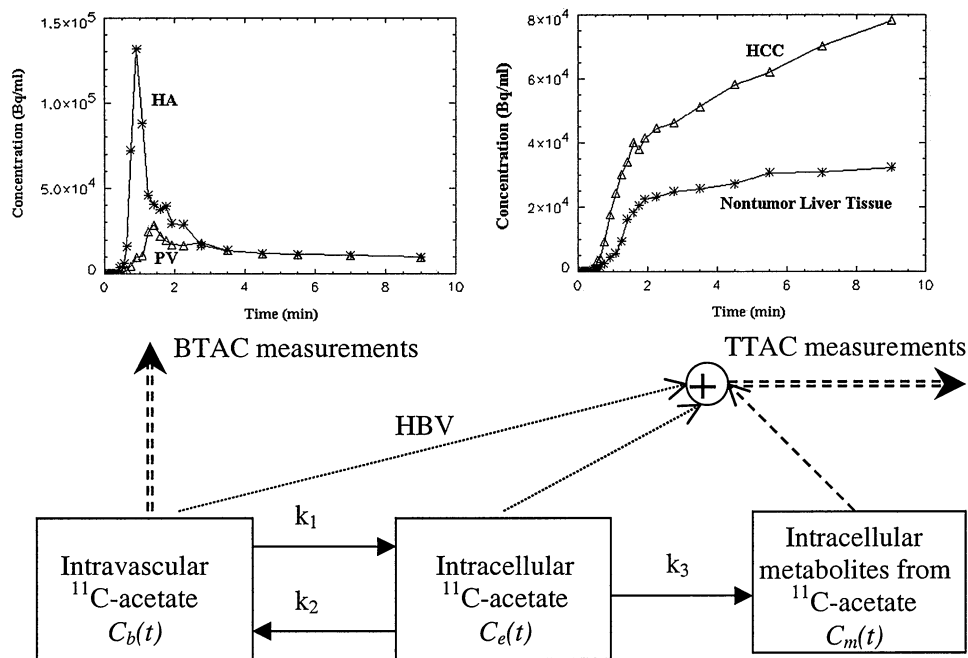$$B_2 = \frac{K_1 k_2}{k_2 + k_3}, \quad L_1 = k_2 + k_3$$

Fig. 1. Three-compartment liver kinetic model for ^{11}C-acetate with an extra parameter in the dual-input function. Typical TACs of HA and PV were illustrated in the BTAC measurements. The last five points of PV measurements were replaced by the corresponding HA data. Solid line marked by an asterisk stands for the HA, triangle for the PV. The greatest activity difference between these two curves is during the early radionuclide angiographic phase. Typical TACs of nontumor liver tissue and HCC were illustrated in the TTAC measurements. Solid line marked by an asterisk stands for the nontumor liver tissue, triangle for the HCC.

are the macroparameters in the ^{11}C-acetate liver model and $\otimes$ denotes the operation of temporal convolution.

In this study, to obtain the proportion of the portal or arterial contribution to the liver blood supply and provide more accurate physiological parameter estimates, a new parameter a_v was included in the model input function to describe the contribution of PV. Therefore, the contribution of HA would be $(1 - a_v)$. Thus, the dual-input function was calculated according to

$$c_b(t) = c_a(t) * (1 - a_v) + c_v(t) * a_v \qquad (6)$$

where $c_a(t)$ is the tracer concentration in the HA and $c_v(t)$ is the tracer concentration in the PV. Substituting $c_b(t)$ in (5) by (6), the equation

$$c_T(t) = (B_1 + B_2 e^{-L_1 t}) \otimes ((1 - a_v) * c_a(t) + a_v * c_v(t)) \\ + \text{HBV} * ((1 - a_v) * c_a(t) + a_v * c_v(t)) \qquad (7)$$

could be obtained.

D. Parameter Estimation and Statistical Analysis

Three-compartment 4P model with parameter a_v in the dual-input function was used to fit the clinical data and compared with the fitting results of the 4P model using fixed weighted dual-input function. With the measurements of $c_a(t)$, $c_v(t)$, and $c_T(t)$ from dynamic PET images, the weighted nonlinear least squares (NLS) algorithm was used to numerically evaluate all of the individual parameters. Model parameters were estimated by minimizing the weighted residual sum of squares (WRSS) [11], which is a direct measurement of the fitting quality. WRSS is given by

$$\text{WRSS}(p) = \sum_{k=1}^{25} w_k [c_T(t_k, p) - z(t_k)]^2 \qquad (8)$$

where p is the vector of parameters to be estimated, w_k is the weight adopted, which is proportional to the length of the scanning interval and inversely proportional to the radioactivity concentration, c_T is the model output, which is a function of p, and z is the PET measurement. The superscript 25 is the total data points to be fitted in this study. LHMRAct could be calculated by

$$\text{LHMRAct} = \frac{K_1 k_3}{k_2 + k_3} \qquad (9)$$

from NLS fitting results.

Patlak analysis [19] was also provided to estimate LHMRAct for the two models to fit the data between 2.5–10 min. Since the Patlak method could not estimate parameter a_v, for the nonfixed weighted dual-input model the input function was calculated according to the estimated value of a_v by using NLS method. The estimated LHMRAct of both models were compared with those obtained from the NLS method, respectively, by correlation analysis.

Apart from WRSS, parameter standard deviation (SD) and coefficient of variation (CV), which are the computed measurements of variability of parameter estimation, were utilized as the statistical criteria. In addition, Akaike Information Criteria (AIC) [20] and Schwarz Criteria (SC) [21] were used to test which model is better. It was assumed that the data variances were known up to a proportionality constant; therefore, the AIC and SC are given by

$$\text{AIC} = N \ln(\text{WRSS}) + 2P \qquad (10)$$
$$\text{SC} = N \ln(\text{WRSS}) + P \ln N \qquad (11)$$

where P is the number of parameters in the model, and N is the number of data points.

TABLE I
ESTIMATED PARAMETERS OF THE THREE-COMPARTMENT 4P ^{11}C-ACETATE
LIVER MODEL WITH 70% CONTRIBUTION FROM PV USING THE NLS METHOD

Datasets number	Rate		constants	
	K_1 (ml/min/ml)	k_2 (min^{-1})	k_3 (min^{-1})	HBV (ml/ml)
1	0.526 ± 0.031	0.221 ± 0.047	0.077 ± 0.040	0.027 ± 0.016
2	0.652 ± 0.049	0.224 ± 0.049	0.043 ± 0.034	0.037 ± 0.021
3	0.700 ± 0.031	0.253 ± 0.029	0.044 ± 0.017	0.015 ± 0.013
4	0.477 ± 0.013	0.259 ± 0.020	0.087 ± 0.013	0.317 ± 0.009
5	0.472 ± 0.026	0.254 ± 0.039	0.077 ± 0.026	0.307 ± 0.018
6	0.730 ± 0.063	0.505 ± 0.081	0.163 ± 0.021	0.271 ± 0.027
7*	1.368 ± 0.113	0.402 ± 0.066	0.104 ± 0.022	0.442 ± 0.054
8	0.880 ± 0.052	0.222 ± 0.038	0.046 ± 0.025	0.081 ± 0.021
9	0.615 ± 0.056	0.283 ± 0.072	0.091 ± 0.042	0.007 ± 0.022
10*	1.185 ± 0.110	0.420 ± 0.117	0.350 ± 0.060	0.234 ± 0.037

* Regions 7 and 10 represent HCC.

TABLE II
ESTIMATED PARAMETERS OF THE THREE-COMPARTMENT 4P ^{11}C-ACETATE
LIVER MODEL WITH 80% CONTRIBUTION FROM PV USING THE NLS METHOD

Datasets number	Rate		constants	
	K_1 (ml/min/ml)	k_2 (min^{-1})	k_3 (min^{-1})	HBV (ml/ml)
1	0.651 ± 0.044	0.306 ± 0.055	0.090 ± 0.030	0.039 ± 0.020
2	0.731 ± 0.064	0.283 ± 0.066	0.064 ± 0.036	0.047 ± 0.027
3	0.760 ± 0.033	0.292 ± 0.032	0.052 ± 0.016	0.035 ± 0.015
4	0.457 ± 0.017	0.237 ± 0.027	0.075 ± 0.020	0.383 ± 0.013
5	0.461 ± 0.034	0.246 ± 0.052	0.072 ± 0.035	0.366 ± 0.023
6	0.651 ± 0.054	0.424 ± 0.071	0.151 ± 0.023	0.367 ± 0.027
7*	1.118 ± 0.054	0.309 ± 0.040	0.107 ± 0.020	0.090 ± 0.023
8	0.907 ± 0.058	0.230 ± 0.042	0.043 ± 0.027	0.162 ± 0.029
9	0.679 ± 0.066	0.290 ± 0.073	0.065 ± 0.039	0.030 ± 0.028
10*	0.657 ± 0.065	0.251 ± 0.171	0.676 ± 0.264	0.070 ± 0.018

* Regions 7 and 10 represent HCC. The input functions of regions 7 and 10
are 100% and 80% contribution from HA respectively.

TABLE III
ESTIMATED PARAMETERS OF THE THREE-COMPARTMENT 4P ^{11}C-ACETATE
LIVER MODEL WITH 85% CONTRIBUTION FROM PV USING THE NLS METHOD

Datasets number	Rate		constants	
	K_1 (ml/min/ml)	k_2 (min^{-1})	k_3 (min^{-1})	HBV (ml/ml)
1	0.687 ± 0.048	0.311 ± 0.055	0.076 ± 0.027	0.063 ± 0.022
2	0.739 ± 0.061	0.280 ± 0.064	0.057 ± 0.037	0.063 ± 0.030
3	0.794 ± 0.035	0.315 ± 0.033	0.056 ± 0.016	0.050 ± 0.017
4	0.449 ± 0.032	0.230 ± 0.047	0.072 ± 0.031	0.415 ± 0.018
5	0.461 ± 0.042	0.252 ± 0.064	0.077 ± 0.043	0.394 ± 0.028
6	0.604 ± 0.049	0.376 ± 0.066	0.142 ± 0.025	0.423 ± 0.026
7*	1.358 ± 0.088	0.405 ± 0.055	0.114 ± 0.019	0.192 ± 0.036
8	0.944 ± 0.063	0.252 ± 0.046	0.050 ± 0.028	0.212 ± 0.034
9	0.762 ± 0.080	0.358 ± 0.084	0.083 ± 0.034	0.052 ± 0.033
10*	0.799 ± 0.067	0.268 ± 0.115	0.460 ± 0.125	0.101 ± 0.021

* Regions 7 and 10 represent HCC. The input functions of regions 7 and 10
are 60% contribution from HA.

TABLE IV
ESTIMATED PARAMETERS OF THE THREE-COMPARTMENT 4P ^{11}C-ACETATE
LIVER MODEL WITH AN EXTRA PARAMETER a_v IN THE DUAL-INPUT
FUNCTION USING THE NLS METHOD

Datasets number	Rate			constants	
	K_1 (ml/min/ml)	k_2 (min^{-1})	k_3 (min^{-1})	HBV (ml/ml)	a_v
1	0.775 ± 0.126	0.360 ± 0.099	0.073 ± 0.025	0.097 ± 0.046	0.913 ± 0.060
2	0.655 ± 0.098	0.238 ± 0.081	0.058 ± 0.042	0.042 ± 0.028	0.700 ± 0.138
3	0.804 ± 0.064	0.323 ± 0.051	0.058 ± 0.017	0.055 ± 0.030	0.863 ± 0.073
4	0.474 ± 0.014	0.256 ± 0.021	0.085 ± 0.014	0.328 ± 0.018	0.717 ± 0.024
5	0.472 ± 0.033	0.255 ± 0.047	0.078 ± 0.028	0.295 ± 0.039	0.675 ± 0.058
6	0.573 ± 0.062	0.350 ± 0.079	0.138 ± 0.030	0.475 ± 0.055	0.899 ± 0.038
7*	1.345 ± 0.170	0.401 ± 0.081	0.115 ± 0.019	0.176 ± 0.092	0.363 ± 0.238
8	0.871 ± 0.098	0.220 ± 0.052	0.049 ± 0.032	0.087 ± 0.051	0.699 ± 0.114
9	0.785 ± 0.160	0.368 ± 0.133	0.080 ± 0.036	0.081 ± 0.080	0.882 ± 0.111
10*	1.022 ± 0.423	0.358 ± 0.223	0.383 ± 0.102	0.160 ± 0.122	0.590 ± 0.270

* Regions 7 and 10 represent HCC.

E. Simulation Study

Computer simulation was also conducted to test the accuracy and reliability of the estimated parameters of the nonfixed weighted dual-input model. The TACs of both PV and HA were extracted from one clinical dataset. The TTAC was calculated according to (4) by using $K_1 = 0.47, k_2 = 0.26, k_3 = 0.09, \text{HBV} = 0.33, a_v = 0.72$. The scanning intervals were the same as those in clinical data acquisition. A pseudorandom number generator was used to generate the Gaussian noise added to the calculated TTAC, and the noise level was set to 0.1, 0.5, and 1.0, respectively. The mean value of the estimated parameters was calculated from 100 simulation runs, and the bias was calculated by

$$\text{Bias} = \left| \frac{P^{\text{true}} - \bar{P}}{P^{\text{true}}} \right| \tag{12}$$

where P^{true} is the true value of the parameter and $\bar{P}$ is the mean value from the NLS fitting results of the computer simulation.

III. RESULTS AND DISCUSSION

The ^{11}C-acetate clinical data of ten ROIs extracted from six patients were analyzed to test the models a with fixed/nonfixed weighted dual-input function. The estimated results of the models with 70%, 80%, and 85% contribution from PV were shown in Tables I–III, respectively. The parameter estimates for the model with a nonfixed weighted input were summarized in Table IV. In Table II, 100% and 80% contribution from HA for regions 7 and 10, respectively, were used; 60% contribution from HA was adopted for regions 7 and 10 in Table III. Comparison of the three groups of estimation results according to CV and WRSS (contained in Table V) was conducted. It could be found that, among the ten datasets, half of the best fitting results are from Table I, whereas the remaining half are almost all from Table III. If the datasets achieving best fitting are from Table I, they always show the worst fitting quality in Table III. On the contrary, if the datasets of best quality are from Table III, they always demonstrate the worst fitting results in Table I. The estimated parameters in Table II exhibit moderate fitting quality.

The estimation results in Table IV demonstrate that the estimated a_v value shows moderate variability among different ROIs from nontumor liver tissue and significant difference between HCC and nontumor regions ($p < 0.05$). Therefore, a nonfixed weighted input function has significant importance to the parameter estimation. The fitting result of a_v is very reliable since the CVs of five ROIs are less than 10%, three are less than 20% and the other two are 65.46% and 45.87%, respectively. The mean value of the estimated a_v for nontumor regions is 0.793, which is comparable with our previous hypothesis and the SD is 0.104. The estimated a_v value of the two HCC ROIs is 0.363 and 0.590, which are much less than those of the nontumor liver tissue. Regarding the comparison stated

TABLE V
COMPARISON OF THE WRSS, AIC, AND SC OF THE MODELS USING A
FIXED/NONFIXED WEIGHTED DUAL-INPUT FUNCTION

Datasets number	WRSS_change (%)			AIC**		SC**	
	Table I	Table II	TableIII	F***	NF***	F	NF
1	62.2	39.7	17.2	180.27	173.91	185.14	180.00
2	-4.5	15.1	23.5	197.40	195.89	202.27	201.98
3	6.1	0.3	-0.1	164.04	165.97	168.92	172.07
4	3.5	84.9	268.5	144.25	130.88	149.13	136.98
5	1.9	42.9	104.5	173.67	166.75	178.55	172.85
6	48.4	25.3	9.8	162.64	158.99	167.51	165.08
7*	8.5	-10.0	1.7	187.95	192.57	192.83	198.67
8	5.2	14.1	19.3	177.67	176.37	182.55	182.46
9	19.9	13.8	2.9	178.76	177.52	183.63	183.61
10*	-4.5	8.5	6.0	169.03	168.98	173.91	175.08

* Regions 7 and 10 represent HCC.
** Comparison of AIC and SC was between the results with the weights in Table II and those with the nonfixed weight.
*** "F" stands for the fixed weight and "NF" stands for the nonfixed weight.

TABLE VI
COMPARISON OF THE CV OF THE ESTIMATED PARAMETERS IN
TABLES II AND IV

Datasets number	K_1 (%)		k_2 (%)		k_3 (%)		HBV (%)		a_v (%)
	F**	NF**	F	NF	F	NF	F	NF	NF
1	6.76	16.21	18.01	27.39	33.17	33.84	52.27	47.91	6.62
2	8.74	15.00	23.34	34.01	56.23	72.34	57.61	65.80	19.72
3	4.38	8.01	10.88	15.69	31.20	29.52	42.88	54.03	8.46
4	3.79	2.97	11.45	8.31	26.82	16.48	3.29	5.50	3.30
5	7.39	6.92	21.08	18.27	48.12	35.41	6.17	13.08	8.59
6	8.35	10.78	16.86	22.60	15.36	21.75	7.33	11.50	4.20
7*	4.87	12.67	12.85	20.07	18.92	16.73	25.19	52.26	65.46
8	6.40	11.23	18.34	23.70	63.00	65.01	17.82	58.06	16.32
9	9.78	20.38	25.29	36.17	59.37	45.75	93.62	98.77	12.55
10*	9.91	41.35	68.11	62.35	39.03	26.64	24.92	76.07	45.87
Average	7.037	14.552	22.621	26.856	39.122	36.347	33.11	48.298	19.109

* Regions 7 and 10 represent HCC.
** "F" stands for the fixed weight and "NF" stands for the nonfixed weight.

in the above paragraph, for every dataset, the most accurate estimation among the three fixed-weight fittings is always with the assumed weight that is closest to the estimated a_v value in Table IV. For example, the estimated a_v value of regions 4 and 5 is 0.717 and 0.675 (shown in Table IV), respectively, for regions 4 and 5, the model with 70% contribution from PV could achieve best fitting quality compared with the other two weight assumptions; the estimated a_v value of region 9 is 0.882 (shown in Table IV), for region 9, the model with 85% contribution from PV could achieve most accurate estimation, which may indicate that the estimated a_v value could be accurate.

The fitting results using the fixed weights in Table II were focused to be compared with those using a nonfixed weighted input model. Compared with the results in Table II, the estimated value of K_1, k_2, k_3 of nontumor regions in Table IV shows no significant difference respectively, which may due to the fact that the estimated a_v value demonstrates relatively less variance from 80%. For nontumor liver tissue, the mean value of K_1 is 0.662 ml/min/ml in Table II and 0.676 ml/min/ml in Table IV; k_2 is 0.288/min in Table II and 0.296/min in Table IV; k_3 is 0.076/min in Table II and 0.077/min in Table IV. However, the fitting results of the two HCC regions exhibit relatively great difference especially for region 10, which may be due to the significant difference between the estimated a_v value and the fixed weight assumed. It could be found that the two sets of estimated HBV value in Tables II and IV differ greatly because HBV is the hepatic blood volume term which is directly affected by the contribution of the hepatic dual inputs. Since the vascularity of a cirrhotic liver is heterogeneous, the estimated HBV value also exhibits moderate variability [5].

Comparison of the WRSS, AIC, and SC of the fixed (weights in Table II)/nonfixed weighted models was conducted, and the results were summarized in Table V. The "WRSS_change" term in Table V was calculated by

$$\text{WRSS\_change} = \frac{\text{WRSS}_F - \text{WRSS}_N}{\text{WRSS}_N} * 100\% \qquad (13)$$

where WRSS_N is the WRSS using a nonfixed input model and WRSS_F is the WRSS using a fixed input model. As shown in Table V, when parameter a_v was used, WRSS (refer to the

second column of WRSS_change) for all regions except region 7 is reduced; all AICs except those of regions 3 and 7 are smaller than those using the fixed weights in Table II, and region 10 shows no obvious improvement; all SCs except those of regions 3, 7, and 10 are smaller, and regions 8 and 9 show no obvious improvement. It could be seen that most cases show that the 4P model plus a weight parameter in the required model input function is the better model to characterize the kinetics of ^{11}C-acetate in the liver especially using AIC as the criteria. Although AIC and SC are very similar, there is no guarantee that they will indicate the same model as the best fit, especially when the number of observations N is large, say more than eight [21], [22]. Therefore, the fitting result of the nonfixed weighted model is satisfactory and parameter a_v could be identified by using the tracer kinetic modeling techniques.

Table VI demonstrates the comparison of the CV of the estimated parameters in Tables II and IV. Although there is one more parameter in the nonfixed weighted input model, the CV value is still acceptable: the mean CV value of the estimated K_1 is 14.552%; k_2 is 26.856%; k_3 is 36.347%; HBV is 48.298%; a_v is 19.109%. About one third of the CVs of the estimated parameters (excluding a_v) even decrease, and the reliability of estimated k_3 is even improved. The model fitted curves according to the fixed/nonfixed weighted input models for two datasets, one from HCC and another from nontumor region, were shown in Fig. 2.

The NLS fitting results of the computer simulation using a nonfixed weighted dual-input model were involved in Table VII. Parameter estimates were expressed as mean ± SD. As seen in Table VII, both the CV and bias of all the estimated parameters from 100 simulation runs are very small, therefore, reliable and accurate parameter estimation of the nonfixed weighted dual-input model could be achieved by using the NLS method.

The ten clinical datasets were also fitted with the Patlak method using the fixed (weights in Table II)/nonfixed weighted dual-input function. Due to the nature of the Patlak method, the data of the early phase (<2.5 min) were not included in the analysis. The results of the estimated forward clearance K for the two models using the NLS and Patlak methods were presented in Table VIII. Since the TACs of the HA and PV are similar after the dynamic phase [11], the estimated K using
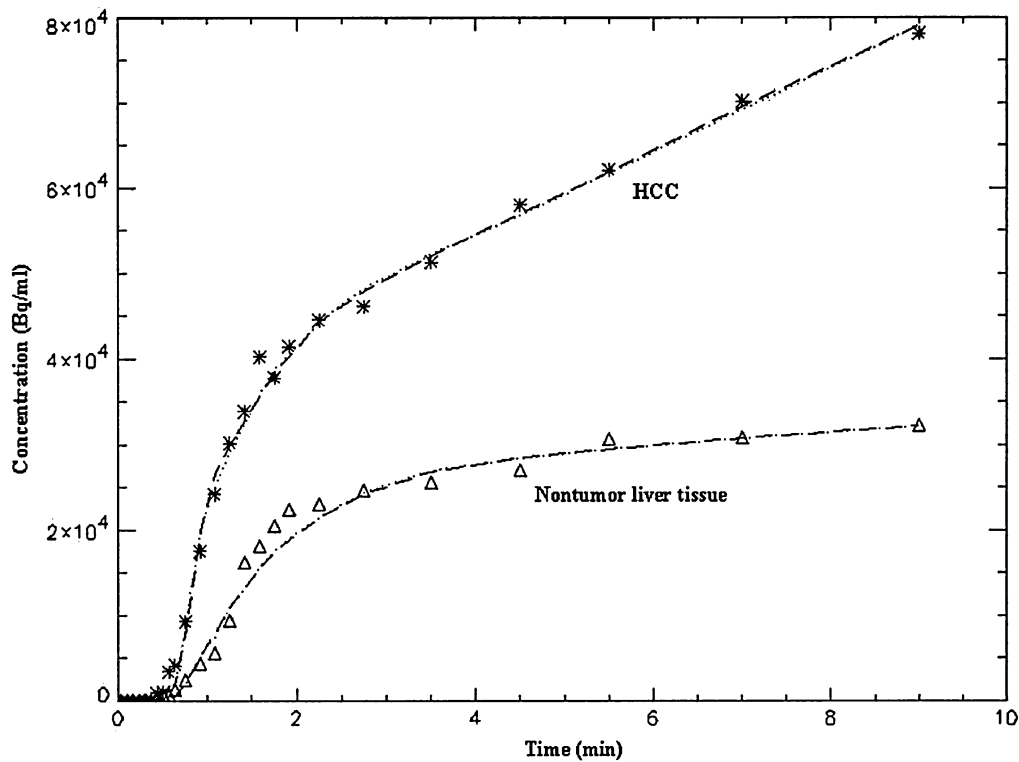
Fig. 2.   Graph shows the generated TACs of the HCC ROI with symbol "*" and the nontumor liver tissue ROI with symbol "$\triangle$." Dashed lines demonstrate the fitting results using the fixed weights (20% and 80% contribution from PV for HCC and nontumor regions, respectively) in the dual-input function; dotted lines stand for the fitting results using an extra parameter in the input function of the ^{11}C-acetate liver model.

TABLE VII
NLS FITTING RESULTS OF THE COMPUTER SIMULATION USING A NONFIXED WEIGHTED DUAL-INPUT MODEL. THE MEAN VALUE, SD, AND BIAS OF $K_1 - k_3$, HBV, a_v, AND K WERE CALCULATED FROM 100 SIMULATION RUNS

Noise level	Rate						constants					
	K_1	Bias	k_2	Bias	k_3	Bias	HBV	Bias	a_v	Bias	K	Bias
0.1	0.4699±0.0034	0.0002	0.2600±0.0045	0.0000	0.0901±0.0023	0.0007	0.3305±0.0050	0.0016	0.7205±0.0067	0.0007	0.1209±0.0016	0.0002
0.5	0.4693±0.0173	0.0015	0.2597±0.0226	0.0011	0.0897±0.0118	0.0028	0.3323±0.0251	0.0071	0.7210±0.0343	0.0014	0.1202±0.0085	0.0054
1	0.4692±0.0352	0.0016	0.2606±0.0454	0.0023	0.0890±0.0231	0.0115	0.3336±0.0500	0.0110	0.7180±0.0703	0.0028	0.1181±0.0176	0.0228

TABLE VIII
ESTIMATED K VALUE FOR THE MODELS WITH FIXED (WEIGHTS IN TABLE II/NONFIXED WEIGHTED DUAL-INPUT FUNCTION USING THE NLS AND PATLAK METHODS, RESPECTIVELY

Datasets number	Estimated K $(K_1*k_3/(k_2+k_3))$			
	NLS method using fixed weighted inputs	Patlak method using fixed weighted inputs	NLS method using non-fixed weighted inputs	Patlak method using non-fixed weighted inputs
1	0.1472	0.1684	0.1305	0.1695
2	0.1341	0.1826	0.1285	0.1770
3	0.1142	0.1548	0.1229	0.1587
4	0.1095	0.1562	0.1183	0.1552
5	0.1050	0.1495	0.1106	0.1480
6	0.1705	0.1611	0.1620	0.1619
7*	0.2883	0.2644	0.2997	0.2686
8	0.1436	0.1836	0.1596	0.1867
9	0.1246	0.1903	0.1397	0.1943
10*	0.4790	0.4711	0.5285	0.5187

* Regions 7 and 10 represent HCC.

the Patlak method is affected less by the input function, and the nonfixed input model shows less difference with the fixed input model. For the eight ROIs from the nontumor liver tissue, the estimated K value expressed as mean±SD with/without a_v is 0.1689±0.0160 and 0.1683±0.0154 ml/min/ml, respectively. For the two ROIs of HCC, the estimated forward clearance K by the Patlak method with/without weight parameter is 0.2686 and 0.2644 ml/min/ml (region 7), 0.5187 and 0.4711 ml/min/ml (region 10). For NLS analysis, the results do show some difference between the two models. For the eight ROIs from the nontumor liver tissue, the estimated K value expressed as mean ± SD with/without a_v is 0.1340±0.0186 and 0.1311±0.0222 ml/min/ml, respectively. For the two ROIs of HCC, the estimated K value with/without weight parameter is 0.2997 and 0.2883 ml/min/ml (region 7), 0.5285 and 0.4790 ml/min/ml (region 10). The correlation coefficients between the estimated K value of the Patlak and NLS methods for the fixed and nonfixed input models are 97.64% and 98.50%, respectively. Just as in [5], the K value of the non-FDG-avid type of HCC (regions 7 and 10) is significantly higher than those of the nontumor liver parenchyma ($p < 0.05$). Therefore, quantitative parametric imaging of LHMRAct may be a potential functional imaging technique to detect HCC.

IV. CONCLUSION

This study suggests that the differential portal and arterial contribution to the liver blood supply could be extracted from the PET dynamic measurements noninvasively using tracer kinetic modeling techniques. The estimated a_v value is reasonable and compatible with the clinical physiological and pathological conditions. It may also add supportive evidence to the viewpoint that liver metastases derive a much greater proportion of their blood supply from the hepatic arterial flow and a smaller proportion from the portal venous flow. In addition, the estimated a_v value might provide useful diagnostic information to improve the early detection of liver tumors due to the fact that the presence of even small liver tumors is associated with subtle changes in the liver blood flow.

The present results show that all of the required parameters can be quantified simultaneously and the parameter estimates are reliable and accurate. The three-compartment 4P model plus an extra weight parameter in the dual-input function is a more appropriate representation of the system and suitable in describing the kinetic characters of ^{11}C-acetate in a 10-min dynamic PET imaging of the liver. It allows more consistent estimation of LHMRAct, which is considered as a potential indicator for evaluating HCC. Therefore, this new model structure and modeling technique can provide a better description of the ^{11}C-acetate kinetic in liver, a better understanding of the blood supply mechanism in liver and, thus, a better method for the early detection of liver cancer.

ACKNOWLEDGMENT

REFERENCES

[1] T. Tobe, H. Kameda, M. Okudaira, M. Ohto, Y. Endo, M. Mito, E. Okamoto, K. Tanikawa, and M. Kojiro, *Primary Liver Cancer in Japan*. Tokyo, Japan: Springer-Verlag, 1992.

[2] T. Tsuzuki, A. Sugioka, and M. Ueda, "Hepatic resection for hepatocellular carcinoma," *Surgery*, vol. 107, pp. 511–520, 1990.

[3] K. T. Watkins and S. A. Curley, "Liver and bile ducts," in *Clinical Oncology*, 2nd ed, M. D. Abeloff, J. O. Armitage, A. S. Lichter, and J. E. Niederhuber, Eds. Harcourt Asia: Science Press, 2000, pp. 1681–1748.

[4] C. Ho, C. Yu, and D. Yeung, "^{11}C-acetate PET imaging in hepatocellular carcinoma and other liver masses," *J. Nucl. Med.*, vol. 44, no. 2, pp. 213–221, 2003.

[5] S. Chen, C. Ho, D. Feng, and Z. Chi, "Tracer kinetic modeling of ^{11}C-acetate applied in the liver with positron emission tomography," *IEEE Trans. Med. Imag.*, vol. 23, pp. 426–432, Apr. 2004.

[6] C. Bartolozzi and R. Lencioni, *Liver Malignancies: Diagnostic and Interventional Radiology*. Berlin, Germany: Springer-Verlag, 1999.

[7] D. L. Morris, C. S. McArdle, and G. M. Onik, *Hepatic Metastases: Diagnosis and Management*. Bath, U.K.: The Bath Press, 1996.

[8] H.-M. Hoogewoud, *Hepatocellular Carcinoma and Liver Metastases: Diagnosis and Treatment*. Berlin, Germany: Springer-Verlag, 1993. A. Rohner.

[9] W. W. Lautt and C. V. Greeway, "Conceptual review of the hepatic vascular bed," *Hepatology*, vol. 7, pp. 952–963, 1987.

[10] W. H. H. Andrews, *Liver*. London, U.K.: Edward Arnold.

[11] O. L. Munk, L. Bass, K. Roelsgaard, D. Bender, S. B. Hansen, and S. Keiding, "Liver kinetics of glucose analogs measured in pigs by PET: Importance of dual-input blood sampling," *J. Nucl. Med.*, vol. 42, no. 5, pp. 795–801, 2001.

[12] C. Breedis and G. Young, "The blood supply of neoplasms in the liver," *Amer. J. Pathol.*, vol. 30, pp. 969–985, 1954.

[13] G. Lin *et al.*, "Postmortem examination of the blood supply and vascular pattern of small liver metastases in man," *Surgery*, vol. 96, pp. 517–526, 1984.

[14] R. Sarper *et al.*, "A noninvasive method for measuring portal venous/total hepatic blood flow by hepatosplenic radionuclide angiography," *Radiology*, vol. 141, pp. 179–184, 1981.

[15] B. C. Chen, S. C. Huang, G. Germano, W. Kuhle, R. A. Hawkins, D. Buxton, R. C. Brunken, H. R. Schelbert, and M. E. Phelps, "Noninvasive quantification of hepatic arterial blood flow with nitrogen-13-ammonia and dynamic positron emission tomography," *J. Nucl. Med.*, vol. 32, no. 12, pp. 2199–2206, 1991.

[16] M. E. Phelps, S. C. Huang, E. J. Hoffman, C. Selin, L. Sokoloff, and D. E. Kuhl, "Tomographic measurement of local cerebral glucose metabolic rate in humans with (F-18)2-fluoro-2-deoxy-D-glucose: Validation of method," *Ann. Neurol.*, vol. 6, pp. 371–388, 1979.

[17] J. Correia, "Editorial: A bloody future for clinical PET," *J. Nucl. Med.*, vol. 33, pp. 620–622, 1992.

[18] S. Chen, L. Wong, and D. Feng, "A new automatic detection approach for hepatocellular carcinoma using ^{11}C-acetate positron emission tomography," in *Proc. IEEE Int. Conf. Image Processing*, Barcelona, Spain, Sept. 14–17, 2003, pp. 1065–1068.

[19] C. S. Patlak, R. G. Blasberg, and J. D. Fenstermacher, "Graphical evaluation of blood-to-brain transfer constants from multiple-time uptake data," *J. Cereb. Blood Flow Metab.*, vol. 3, pp. 1–7, 1983.

[20] H. Akaike, "A new look at the statistical model identification," *IEEE Trans. Automat. Control*, vol. AC-19, pp. 716–723, Dec. 1974.

[21] G. Schwarz, "Estimating the dimension of a model," *Ann. Stat.*, vol. 6, pp. 461–564, 1978.

[22] A. B. Koehler and E. S. Murphee, "A comparison of the Akaike and Schwarz criteria for selecting model order," *Appl. Stat.*, vol. 37, pp. 187–195, 1988.

Sirong Chen was born in China in May 1977. She received the B.Eng. degree in biomedical engineering from Tianjin University, Tianjin, China, in 2000. She is currently working toward the Ph.D. degree at Hong Kong Polytechnic University.

From August 2000 to May 2002, she worked as a Research Assistant with the Department of Electronic and Information Engineering, Hong Kong Polytechnic University. Her research interests include quantitative functional imaging with positron emission tomography, modeling and simulation, and fast algorithms.

Dagan Feng (M'88–SM'94–F'02) was born in Nanking, China. He received the M.E. degree in electrical engineering and computer science from Shanghai JiaoTong University, Shanghai, China, in 1982, and the M.Sc. degree in biocybernetics and the Ph.D. degree in computer science from the University of California, Los Angeles, in 1985 and 1988, respectively.

After briefly working as an Assistant Professor in the United States, he joined the University of Sydney, Sydney, Australia, as a Lecturer, Senior Lecturer, Reader, and then Professor. He is the former Head of the Department of Computer Science/School of Information Technologies. He is currently Associate Dean of the Faculty of Science and Director of the Biomedical & Multmedia Information (BMIT) Research Group, University of Sydney, and Chair-Professor of Information Technology, Center for Multimedia Signal Processing, Department of Electronic and Information Engineering, Hong Kong Polytechnic University. He has published over 300 scholarly research papers, pioneered several new research directions, and made a number of landmark contributions in his field. More important, however, is that many of his research results have been translated into solutions to real-life problems and have made tremendous improvements to the quality of life worldwide.

Prof. Feng is a Fellow of the American Chemical Society, the Hong Kong Institute of Engineering, the Insitute of Electrical Engineers and is currently chairman of IFAC-TC-BIOMED. He was the recipient of the Crump Prize for Excellence in Medical Engineering.